Coupled channel analysis of proton scattering from ^{40}Ar

R. De Leo
Dipartimento di Fisica dell'Universita'di Bari, Bari, Italy
and Istituto Nazionale di Fisica Nucleare, Sezione di Bari, Italy

S. Micheletti and M. Pignanelli
Dipartimento di Fisica dell'Universita'di Milano, Milano, Italy
and Istituto Nazionale di Fisica Nucleare, Sezione di Milano, Italy

M. N. Harakeh
Kernfysisch Versneller Instituut, Groningen, The Netherlands
(Received 28 September 1984)

Angular distributions for the elastic and inelastic scattering of 29.6 and 35.1 MeV protons from the 0_1^+ (g.s.), 2_1^+ (1.461 MeV), 0_2^+ (2.121 MeV), 2_2^+ (2.524 MeV), 4_1^+ (2.893 MeV), 2_3^+ (3.208 MeV), 3_1^- (3.681 MeV), and 2_4^+ (3.919 MeV) states in ^{40}Ar have been measured. Coupled channel calculations for the 0_1^+, 2_1^+, and 4_1^+ levels have been performed in the framework of the rigid-rotor and harmonic vibrator models. Both analyses give satisfactory descriptions of the data with slight differences in the values of the deformation parameters. Two different analyses have been performed for the 0_2^+ and 2_2^+ levels. In the first, they have been considered as belonging to the β band and analyzed using the rotor-vibrator model. In the second, the coupling strengths between the various states have been treated as free parameters not linked to rigid ratios from models. The intrinsic quadrupole moment of the β band extracted from the two analyses is in agreement with that deduced from γ-decay studies. The distorted wave Born approximation has been used for the analysis of the 3_1^- level. The 3_1^-, 2_3^+, and 2_4^+ levels have also been analyzed with different coupled channel calculations in which their coupling amplitudes to the ground state and 2_1^+ state have been adjusted as free parameters.

I. INTRODUCTION

The coexistence of spherical and deformed states in magic and doubly magic nuclei is well known. Typical examples in the calcium region are given by ^{40}Ca (Refs. 1 and 2), ^{42}Ca, and ^{38}Ar (Refs. 3–5). Recently the phenomenon has been evidenced also in ^{40}Ar (Ref. 6). Its low-lying level structure shows a strong analogy with that of ^{42}Ca and has therefore been considered[6] as formed from the weak coupling of the low-lying levels of the latter with two $d_{3/2}$ proton holes. These are coupled to $L=0$ in the lowest excited levels. The 2^+ (3.208 MeV) level results from the coupling of the two proton holes in the $L=2$ configuration with the ^{42}Ca ground state, while the coupling of the two proton holes in the $L=2$ configuration with the first excited state of ^{42}Ca generates a pentad of levels with $0\leq I\leq 4$, centered about 1.52 MeV (energy of the first 2^+ state in ^{42}Ca) above the 2^+ (3.208 MeV) level. The coupling between the two proton holes and ^{42}Ca levels is weak so that it leaves the electromagnetic (em) transition rates in the ^{40}Ar daughter nucleus very similar to those of the parent ^{42}Ca. A more striking phenomenon is that the ratios among the excitation energies of the first excited states in both nuclei are also similar, indicating that the coupling between the two proton holes and the different excited levels of ^{42}Ca occurs approximately with the same interaction energy.

In analogy with ^{42}Ca, the low-lying levels of ^{40}Ar can be grouped into two bands: (i) the spherical ground state (g.s.) band which results from the coupling of two $f_{7/2}$ neutrons with the $L=0$ $(\pi d_{3/2})^2$ configuration, and (ii) a deformed rotational band (β band) with the bandhead being the 0_2^+ state at 2.121 MeV. The deformed band has been evidenced[6] in ^{40}Ar through the strong 4_2^+ (3.515 MeV)$\rightarrow 2_2^+$ (2.524 MeV) and 6_2^+ (4.958 MeV)$\rightarrow 4_2^+$ (3.515 MeV) $E2$ transitions. From these transitions an intrinsic quadrupole moment of $Q_0=1320$ e mb has been estimated for the β band. Unfortunately, the 2^+ (2.524 MeV)$\rightarrow 0^+$ (2.121 MeV) γ transition, the most important for a complete characterization of the band, has not been observed[6] due to the small energy separation between the two levels.

The aim of this work is to evaluate the intrinsic quadrupole moment Q_0 for the β band from a coupled channel (CC) analysis of proton inelastic scattering to levels of the g.s. and β bands, including the 0^+ and 2^+ levels of the β band. The reliability of our results is dependent on how far the β band could be described as an ideal rotational band and is also linked to the extent to which we are able to reproduce hadron scattering differential cross sections of excited 0^+ levels. The latter problem is notoriously difficult because the form factors of $\lambda=0$ transitions, the assignment of the excited 0^+ states to a band structure, the reduced matrix elements (rme),[7] and the relative phases for all the multipolarities of the different transitions are not yet well known.

Recently encouraging results[8,9] in the reproduction of the β-band cross sections were obtained in the framework

of the rotor-vibrator model,[10] in which all of the preceding quantities follow from the coupling of a vibration to a static deformation. To reach our aim, proton scattering from ^{40}Ar has been measured at 29.6 and 35.1 MeV, energies sufficiently high to avoid compound nucleus contributions to the data. Detailed information on the experimental apparatus is given in Sec. II. The optical model parameters for ^{40}Ar have been deduced from the analysis of the spherical levels 0_1^+ (g.s.), 2_1^+ (1.461 MeV), and 4_1^+ (2.893 MeV). This is reported in Sec. III. Unfortunately, the level scheme of ^{40}Ar is such that the 4^+ level at 3.515 MeV, third level of the β band, could not be resolved from its neighbor at 3.511 MeV. Therefore our evaluation of Q_0 for the β band is limited to only the $0^+ \rightarrow 2^+$ transition, just the one missed in γ-decay experiments. This evaluation is described in Sec. IV. The 3_1^- (3.681 MeV) cross sections are analyzed in Sec. V, and the transitions to the 2^+ levels at 3.208 and 3.919 MeV are examined in Sec. VI. The conclusions are summarized in Sec. VII.

II. EXPERIMENTAL PROCEDURE

The cross sections presented in this paper were taken at incident proton energies of 29.6 and 35.1 MeV using the analyzed beam from the Milan AVF cyclotron. A gaseous ^{40}Ar target at the pressure of 300 Torr was used; the gas was contained in a cylindrical brass case with windows covered with a 1 μm thick kapton foil. The thickness of the target was estimated by its pressure. Scattered protons were detected by three telescopes of 2000 and 5000 μm surface-barrier silicon detectors. The angular distributions were taken in steps of 5° from 10° to 170° in the laboratory system.

The overall energy resolution of the spectra, which includes incident beam energy spread, kinematic and target thickness broadening, and electronics noise, varied from 80 to 120 keV. A typical spectrum, taken at the incident energy of 29.6 MeV and $\theta_{lab}=115°$, is shown in Fig. 1. Levels for which cross sections have been determined are the 0_1^+ (g.s.), 2_1^+ (1.461 MeV), 0_2^+ (2.121 MeV), 2_2^+ (2.524 MeV), 4_1^+ (2.893 MeV), 2_3^+ (3.208 MeV), 3_1^- (3.681 MeV), and 2_4^+ (3.919 MeV) levels. These are labeled with their excitation energies in Fig. 1. The levels 6_1^+, $(1,2)^+$, and 4_2^+, closely spaced around 3.5 MeV excitation energy, were not resolved.

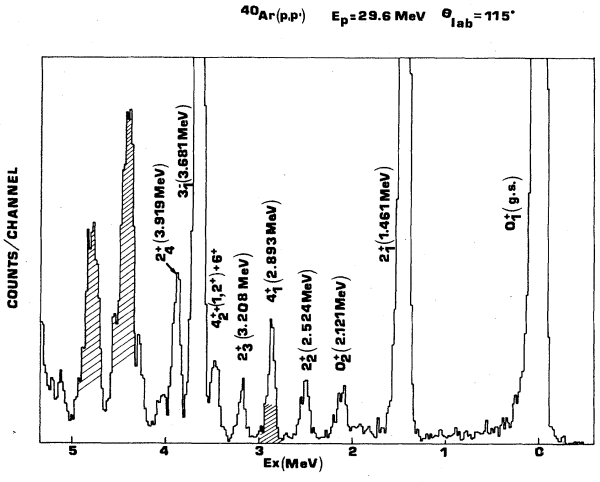

FIG. 1. A typical ^{40}Ar spectrum; levels are labeled by J^π and excitation energy. Hatched peaks are due to contaminants.

Absolute cross sections were determined from target thickness, collected charge, and solid angle measurements. Considering all the uncertainties, including those due to target thickness, collected charge, and solid angle, the systematic error in the cross section's absolute values (not shown in the figures) is less than 10%. Only the statistical error, when larger than data point dimension, is shown in the figures. Numerical values of measured cross sections are reported in Ref. 11.

III. SPHERICAL STATES ANALYSIS

Two analyses have been performed for the 0_1^+ (g.s.), 2_1^+ (1.461 MeV), and 4_1^+ (2.893 MeV) g.s. band states. From the first analysis, performed in the framework of the harmonic vibrational model, optical model potentials (OMP) used in the subsequent analyses were obtained. Averaged values of optical model parameters deduced from analyses of elastic cross sections at different energies between 20 and 40 MeV already exist in the literature;[12] they are reported for quick reference in Table I. We have retained the same values for the geometrical parameters and readjusted the well depths. The results obtained are listed in the third and fourth columns of Table I for the two incident energies, respectively. The obtained phonon amplitudes are reported in Table II. A good reproduction of the data has been obtained, as shown with full lines in Figs. 2 and 3 for the two incident energies, respectively. In this calculation the 4_1^+ state has been considered as formed by the mixing of a hexadecapole phonon and a two-quadrupole phonon component through the 2_1^+ state. The value of the mixing angle, reported in Table II, indi-

TABLE I. Optical model parameters for protons of energy E scattered from ^{40}Ar in the usual notation (depths in MeV and lengths in fm). In the second column, values from Ref. 12 have been reported.

E	21–49	29.6	35.1
V_0	$59.1-0.3E$	51.3	47.8
r_0	1.14	1.14	1.14
a_0	0.75	0.75	0.75
W_v	$0.23E-4.0$	3.65	2.73
W_s	$10.0-0.156E$	4.81	4.45
r_0	1.3	1.3	1.3
a_w	0.66	0.66	0.66
V_{so}	4.45	5.04	4.56
r_{so}	1.01	1.01	1.01
a_{so}	0.56	0.56	0.56
r_C	1.2	1.2	1.2

TABLE II. ^{40}Ar deformation parameters as deduced from the analyses in the present paper.

	Vibrational model analysis[a]	Rotational model analysis[b]	Rotor-vibrator model analysis[c]	Rotor-vibrator model analysis[d]	DWBA analysis[e]
β_2	0.242±0.005	0.220±0.004	0.220[f]	0.220[f]	
β_4	0.107±0.012	0.078±0.007	0.078[f]	0.078[f]	
θ	21°±19°				
$\lvert\beta-\beta_2\rvert$			0.211±0.042	0.061±0.012	
β_0			0.032±0.008	−0.029±0.008	
β_2^β				0.332±0.030	
β_3					0.260±0.030

[a]In Sec. III.
[b]In Sec. III.
[c]In Sec. IV. Levels coupled: 0_1^+, 2_1^+, 0_2^+.
[d]In Sec. IV. Levels coupled: 0_1^+, 2_1^+, 0_2^+, 2_2^+.
[e]In Sec. V.
[f]Parameters kept fixed.

cates that the state is predominantly of one-phonon character.

From the second analysis, performed using the rotational model, quadrupole and hexadecapole deformation parameters to be used in the next sections have been deduced. The values obtained are reported in Table II. The fits obtained are similar to those obtained using the harmonic vibrational model and thus not reported in the figures. It should be stressed that the use of the rotational model is in contrast with the hypothesis of sphericity for the levels involved.

A special insight into the results of the models can be

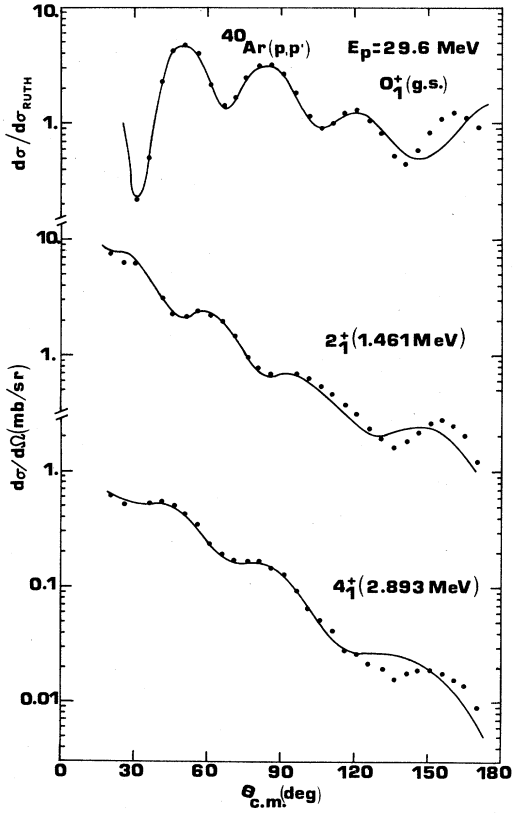

FIG. 2. Differential cross sections (dots) of the ^{40}Ar 0_1^+, 2_1^+, and 4_1^+ levels at the incident proton energy of 29.6 MeV. The full curves are the results of a coupled channel analysis in the framework of the vibrational model. Optical model parameters from Table I and deformations from Table II have been used.

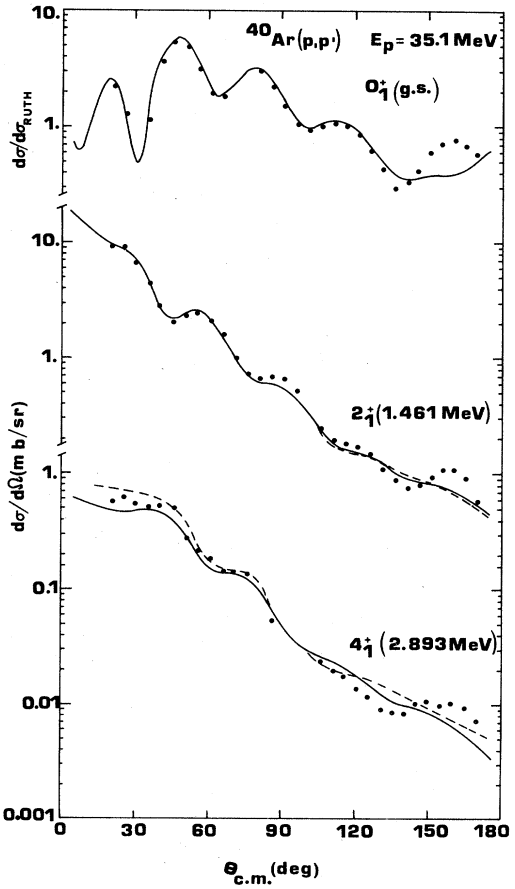

FIG. 3. Data and curves same as in Fig. 2 for protons of 35.1 MeV. The dashed curves have been obtained using the rme values in the seventh row of Table IV.

obtained by comparing the potential radial moments for the different transitions. These have been evaluated for the vibrational model with the formula:

$$M(E\lambda)(\mathrm{p,p'})=\frac{Z\int V_{\mathrm{trans}}r^{\lambda+2}dr}{4\pi\int V_{\mathrm{opt}}r^{2}dr}\times\mathrm{rme}\ (e\ \mathrm{fm}^{\lambda})\ , \qquad (1)$$

and are related to the reduced transition probabilities by

$$B(E\lambda,J_1\rightarrow J_2)(\mathrm{p,p'}) = |M(E\lambda)(\mathrm{p,p'})|^2/(2J_1+1)(e^2\ \mathrm{fm}^{2\lambda})\ . \qquad (2)$$

Note that the preceding definition of $M(E\lambda)(\mathrm{p,p'})$ results from the definition of the isoscalar mass multipole transition operator as:

$$(Z/A)\sum_{\mathrm{nucleons}} r^{\lambda}Y^{\lambda}\ .$$

This is defined in this manner to ensure that for isoscalar collective excitations, where protons and neutrons contribute to the isoscalar transition matrix element in the ratio (Z/A), transition rates obtained from γ decay and inelastic hadron scattering are the same.

In the framework of the vibrational model,[7] the rme term in Eq. (1) is the product of the λ-pole deformation of the nucleus and the matrix element $\langle J_1||Q||J_2\rangle$ evaluated by the code ECIS;[13] in such a case well-fixed relations exist between the rme values of different transitions. In the case of the rotational or rotor-vibrator models where V_{opt} and V_{trans} are deformed, the multipole moments [Eq. (1)] were calculated using the program BEL.[10]

The potential moments can be compared with the corresponding quantities obtained from γ-decay experiments. The γ-decay scheme of low-lying levels of ^{40}Ar is reported in Table III. It contains the information on branching ratios, mixing ratios, and lifetimes from the systematics of Endt and van der Leun,[14] and from the work of Bitterwolf *et al.*[6] Some mixing ratios have been taken from Ref. 15. From the data in Table III we have evaluated the reduced transition probabilities $B(E\lambda)$(em) that we have reported in the third and fourth columns of Tables IV, V, and VII.

The $B(E\lambda)$ deduced from γ decay are due only to proton matrix elements of the collective transition densities, while those from a (p,p') experiment are due also to neu-

TABLE III. Gamma-ray branching ratio, mixing ratios (in parentheses), and lifetimes (τ_m) for the levels of ^{40}Ar studied in the present paper.

J_i	E_x (MeV)	J_f	$0^+_{g.s.}$	2^+_1	0^+_2	2^+_2	4^+_1	τ_m (fs)	Ref.
			59±3	21±2	12±1	8±1	<2	440±90	14
2^+_4	3.919		60±4	18±2	9±2	13±2		400±50	6
			(>0.3, <6)						15
			<5	85±3	<5	<6	15±3	140±80	14
3^-_1	3.681			86±2		4±5	10±1	190±40	6
				(0.07±0.11)					15
				60±2		9±5	31±2	200±40	6
4^+_2	3.515						(0.07±0.1)		6
$1^+,2^+$	3.511		14±2	81±3		5±1		70±20	6
							100	980000±30000	14
6^+_1	3.464						100	>4000	6
			11±2	89±2	<2	<2	<1	45±10	14
2^+_3	3.208		10±1	90±1				40±20	6
				(−0.11±0.07)					15
			<1	100	<1	<1		4300±1500	14
4^+_1	2.893			100				3200±800	6
			41±2	59±2	<1			300±40	14
2^+_2	2.524		43±1	57±1				390±60	6
				(0.33±0.09)					14
			<1	100				130000±40000	14
0^+_2	2.121			100				>4000	6
			100					1600±60	14
2^+_1	1.461		100					2000±40	6

TABLE IV. $B(E\lambda)$ values in $e^2\text{fm}^{2\lambda}$ from γ-decay experiments and from the (p,p′) analyses described in Sec. III.

$J_1 \to J_f$	λ	$B(E\lambda)$(em)[a]	$B(E\lambda)$(em)[b]	$B(E\lambda)$(p,p′)[c]	$B(E\lambda)$(p,p′)[d]	$B(E\lambda)$(p,p′)[e]	$B(E\lambda)$(p,p′)[f]
$0_1^+ \to 2_1^+$	2	384±14	307±6	458±80	430±10	441±10	447±10
$0_1^+ \to 4_1^+$	4			113234±5860	77458±10850	79992±5470	79992±5470
$2_1^+ \to 4_1^+$	2	57±20	77±19	236±41	40±1	54±22	135±37
$2_1^+ \to 4_1^+$	4			29411±1330	0	63040±37260	4697±9086

[a]Deduced from Ref. 14.
[b]Deduced from Ref. 6.
[c]From the rotational analysis.
[d]From the vibrational analysis.
[e]From a fit on the rme's. Reorientation terms fixed at values from analysis of the fifth column. First derivative ($\lambda=2,4$) form factors.
[f]From a fit on the rme's. Reorientation terms fixed to zero. First derivative ($\lambda=2,4$) form factors.

trons. A ratio $B(\text{p,p}')/B(\text{em})$ greater (smaller) than one means[16] that in the considered transition the neutron contribution is larger (smaller) than that of the protons. These comparisons are significant only if in the (p,p′) analysis all the relevant channels for the transition under consideration have been taken into account. Such dispersive effects are, on the contrary, not important for electromagnetic probes.

The $B(\text{p,p}')$ deduced from the two previous analyses are reported in the fifth (rotational model) and sixth (vibrational model) columns of Table IV. The quoted uncertainties reflect the correlation errors due to the fact that several parameters have been put in search, and the averaging procedure used for the values obtained at the two incident energies. The sign in front of each $B(\text{p,p}')$ is that of the corresponding multipole moments $M(\text{p,p}')$ [Eq. (1)] which determines the phase of each contribution in the coupled channel analysis. In Table IV there is clear evidence that, for the $0^+ \to 2^+$ transition, the $B(E2)$ deduced from (p,p′) analyses is larger than that from (em) experiments. The fact that this transition seems to be dominated by neutron contributions confirms the hypothesis that the lowest excited states of ^{40}Ar are due to the recoupling of two neutrons in the $f_{7/2}$ shell. No comparison between the $B(E4)$ evaluated in (p,p′) and (em) analyses can be done for the lack of the latter data. The $B(E\lambda)$(p,p′) obtained from the vibrational model for all the transitions are smaller than those from the rotational model. This reflects the absence in the former of the reorientation terms and of an $L=4$ transition in the $2^+ \to 4^+$ channel.

Two further analyses have been performed for these levels leaving the ($\lambda=2$, $0^+ \to 2^+$), ($\lambda=4$, $0^+ \to 4^+$), ($\lambda=2$, $2^+ \to 4^+$), and ($\lambda=4$, $2^+ \to 4^+$) rme values free to vary from their model values. In the first analysis the reorientation terms were included and fixed to values obtained from the rotational model analysis; in the second analysis these terms were excluded (as they should be for spherical levels). In both analyses, however, first derivative form factors were used. The fits obtained in the two analyses are similar, and thus only those from the first are reported with dashed lines in Fig. 3. The $B(E\lambda)$(p,p′) values obtained are reported in the seventh and eighth columns of Table IV, respectively. Comparing the fits in

TABLE V. $B(E\lambda)$ values ($\lambda=2,4$ in $e^2\text{fm}^{2\lambda}$, $\lambda=0$ in $e^2\text{fm}^4$) from γ-decay experiments and from the (p,p′) analyses described in Sec. IV.

$J_i \to J_f$	λ	$B(E\lambda)$(em)[a]	$B(E\lambda)$(em)[b]	$B(E\lambda)$(p,p′)[c]	$B(E\lambda)$(p,p′)[d]	$B(E\lambda)$(p,p′)[e]	$B(E\lambda)$(p,p′)[f]
$0_1^+ \to 2_1^+$	2	384±14	307±6	458±80	458±80	459±19	448±20
$0_1^+ \to 0_2^+$	0			0.16±1.1	−45±10	−12.4±8.7	
$2_1^+ \to 0_2^+$	2	10±3.1	<325	46±17	−7.8±1.4	−1.4±0.4	
$0_1^+ \to 2_2^+$	2	55±7.3	44.2±6.8		−39±7.2	−35±0.2	24±2
$2_1^+ \to 2_2^+$	0				−2.9±0.6	−23.5±2.7	
$2_1^+ \to 2_2^+$	2	118±16	87±13		11±2	−1.3±1.1	0.6±1.4
$2_1^+ \to 2_2^+$	4				−479±119	−7889±750	−4697±4130
$0_2^+ \to 2_2^+$	2	<12790			971±91	2277±364	

[a]Deduced from Ref. 14.
[b]Deduced from Ref. 6.
[c]From the rotor-vibrator analysis coupling the 0_1^+, 2_1^+, and 0_2^+ levels.
[d]From the rotor-vibrator analysis coupling the 0_1^+, 2_1^+, 0_2^+, and 2_2^+ levels.
[e]From a fit on the rme's. First derivative ($\lambda=2,4$) and Satchler ($\lambda=0$) form factors. 0_1^+, 2_1^+, 0_2^+, and 2_2^+ levels coupled.
[f]From a fit on the rme's. First derivative ($\lambda=2,4$) form factors. 0_1^+, 2_1^+, and 2_2^+ levels coupled.

Fig. 3 we note that the dashed lines, obtained with a larger number of free parameters, reproduce the data only slightly better; no relevant gain in this respect is obtained relaxing the model constraints. As a conclusion of this section we remark that the spherical levels data can be equally well reproduced by the rotational and the vibrational models; differences in the values of the deduced multipole moments connecting to the g.s. have been found to be small (see Table IV).

IV. BETA-BAND LEVEL ANALYSES

Levels in the β band have been analyzed in terms of the rotor-vibrator model[10] which recently proved successful in fitting the levels of the β bands in ^{24}Mg and ^{12}C (Refs. 8 and 9). In this model,[10] the radius of the nucleus is expressed as the sum of a β vibration and of a static deformation (β_2,β_4). All the g.s. band members (here only the 0_1^+ and 2_1^+ have been considered) are coupled to the levels of the β band, with the following form factors:

$$f_{\lambda 0\lambda}(r)=(-1)^{\lambda}\langle I_\beta 0\lambda 0\,|\,I_g 0\rangle\frac{1}{\sqrt{4\pi}\hat{\lambda}}\sum_l \hat{l}v_l^{(1)}(r)(\sqrt{5}\,|\,\beta-\beta_2\,|\,\langle l020\,|\,\lambda 0\rangle^2-\xi\langle l000\,|\,\lambda 0\rangle^2)\,. \tag{3}$$

(See Refs. 8–10 for further details concerning these form factors.)

All the multipolarities are weighted by $|\beta-\beta_2|$, that is the quadrupole amplitude of the β vibration. The multipolarity $\lambda=0$ form factor is similar in shape to that given by the diffuseness monopole vibrator of Satchler[17] with the node shifted to a slightly smaller radius; the $\lambda=2$ to a first derivative form factor with the maximum shifted to a slightly larger radius. The couplings within a rotational band are described by deformed form factors derived from the optical potentials with respective deformations β_2 and β_2^β for the g.s. and the β bands. The quadrupole deformation parameter β_2^β of the β band constitutes the aim of this analysis.

The description of the excitation of the low-lying 0^+ states is complicated[18,19] by the mixing of the giant monopole resonance (GMR). For heavy nuclei where the GMR is known, it is possible to calculate[18] the effective charge for monopole transitions resulting from such a mixing, whereas in light nuclei, where only a small percentage of the $E0$ monopole strength has been located,[20] this is not possible. However, the mixing of the GMR into the low-lying 0^+ states can be represented by an additional coupling to the g.s. which is assumed to have the compressional monopole form factor of Satchler.[17]

The rotor-vibrator model calculations have been performed with a modified version[10] of the code CHUCK.[21] In a preliminary analysis we assumed $\beta_2^\beta=0$. A search on the parameters β_0 and $|\beta-\beta_2|$ resulted in the values in Table II and the long-dashed line fit of Fig. 4. Even if the calculated curve does not show the steep rise at small angles, typical of a $\lambda=0$ multipolarity, the fit is of good quality for a 0_2^+. But the obtained β-vibrational amplitude $|\beta-\beta_2|$ is not realistic since it is a large fraction of the static quadrupole deformation. The $B(E\lambda)$ values deduced from this analysis are shown in the fifth column of Table V. The $B(E0,0_1^+\rightarrow 0_2^+)$ (to our knowledge no experimental result from em studies exists for this quantity) is obtained summing the two monopole potential moments and is too small compared to similar values in this mass region. The $B(E2,2_1^+\rightarrow 0_2^+)$(p,p') is in agreement with the upper limit of Bitterwolf *et al.*[6] (fourth column), but is too high compared with the systematics of Endt and van der Leun[14] (third column).

Subsequently, the 2_2^+ level was also included in the CC scheme, and a search on the parameters β_0, $|\beta-\beta_2|$, and β_2^β was performed at both energies. The results are reported in Table II, the fits in Figs. 4 and 6 with full lines, and the $B(E\lambda)$ values in the sixth column of Table V. The fits of the 2_2^+ cross sections are good. The 0_2^+ curves so evaluated reproduce the peaked shape at 0°, but the experimental bump around 40° in the 29.6 MeV cross section is underestimated. The resulting $|\beta-\beta_2|$ is now only 25% of the static quadrupole deformation and the β_0 and $|\beta-\beta_2|$ values have opposite signs. Their interference results in a $B(E0,0_1^+\rightarrow 0_2^+)$ value of 45 e^2fm^4 corresponding to $\sim 1\%$ of the monopole energy weighted sum rule.

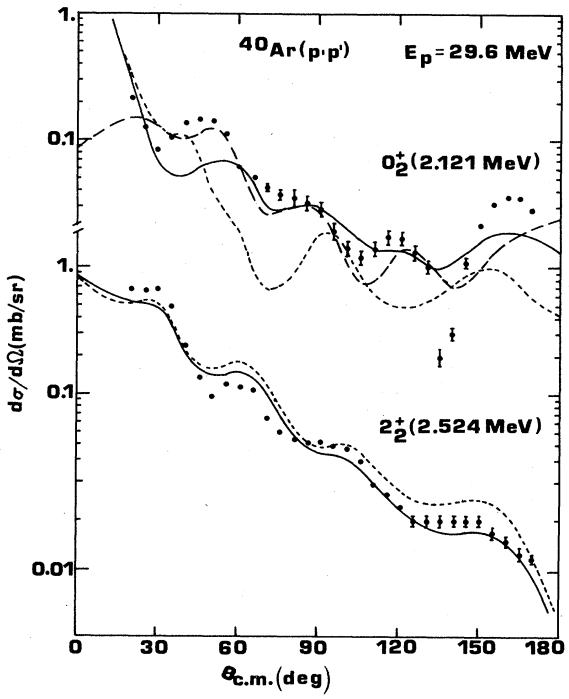

FIG. 4. Cross sections of the 0_2^+ and 2_2^+ levels of ^{40}Ar at the incident proton energy of 29.6 MeV. The curves are the results of a rotor-vibrator model analysis, coupling the 0_1^+, 2_1^+, 0_2^+, and 2_2^+ levels (full lines). The short-dashed lines have been obtained omitting the $0_2^+\rightarrow 2_2^+$ coupling; the long-dashed line is obtained omitting the 2_2^+ level from the coupling scheme.

The $B(E2)$ values for the $(0_1^+ \rightarrow 2_2^+)$ and $(2_1^+ \rightarrow 0_2^+)$ transitions now have values very similar to those from (em) experiments, while the $B(E2,2_1^+ \rightarrow 2_2^+)$ is smaller. The β_2^β obtained from this analysis corresponds to an intrinsic quadrupole moment of $Q_0 = 988 \pm 90$ e mb in good agreement with the values reported by Bitterwolf *et al.*[6] from the $6^+ \rightarrow 4^+$ and $4^+ \rightarrow 2^+$ cascades: $1320(+60, -120)$ e mb.

To investigate the influence of the $0_2^+ \rightarrow 2_2^+$ contribution, we have omitted this coupling in the 29.6 MeV calculations. A strong effect on the 0_2^+ is evident as shown by the short-dashed curves in Fig. 4. This indicates its importance for reproduction of both the absolute value and the shape of the 0_2^+ cross section. The same coupling causes a minor effect on the 2_2^+ cross section.

A further analysis of the 0_2^+ and 2_2^+ levels has been performed keeping the same coupling scheme but abandoning the rotor-vibrator model. We assumed first derivative form factors for the $\lambda = 2$ and 4 multipolarities; for monopole transitions both Satchler[17] form factors were considered, the compressional one acting only in the $0_1^+ \rightarrow 0_2^+$ transition. It is interesting to note that both of Satchler's $\lambda = 0$ form factors have their nodes approximately at the same radial distance, thus their interference can hardly result in a monopole form factor with two nodes. A combination of the β-vibrational form factor with the breathing mode form factor can, on the other hand, produce such a two-nodal monopole form factor. In this case, the distance between these two nodes is dependent on the deformation of the nucleus. The multipole moment of each multipolarity is considered as a free parameter and not linked, as in the framework of the models, to those of other transitions. The results of this analysis are reported in the seventh column of Table V and the fits in Figs. 5 (full lines) and 6 (long-dashed lines) for the two incident energies, respectively. These fits are of the same quality as those from the previous analysis but some of the $B(E\lambda)$ values are now far from their corresponding (em) values, in particular, the $B(E2,2_1^+ \rightarrow 2_2^+)$ value is now much smaller than its corresponding em value. The increased $B(E2,0_2^+ \rightarrow 2_2^+)$ value results in $Q_0 = 1521 \pm 444$ e mb for the intrinsic quadrupole moment of the β band which, notwithstanding its increase with respect to the value obtained from the last analysis, is still in agreement, within the uncertainties, with all the other values.

A last analysis similar to the previous one, but coupling only the 0_1^+, 2_1^+, and 2_2^+ levels, was performed to check the importance of the coupling between the 0_2^+ and the 2_2^+ in the determination of the $B(E2)$ value connecting the 2_2^+ level to the g.s. The 2_2^+ fits are displayed in Figs. 5 and 6 with short-dashed lines and the evaluated $B(E\lambda)$ value in the eighth column of Table V. The fits for the

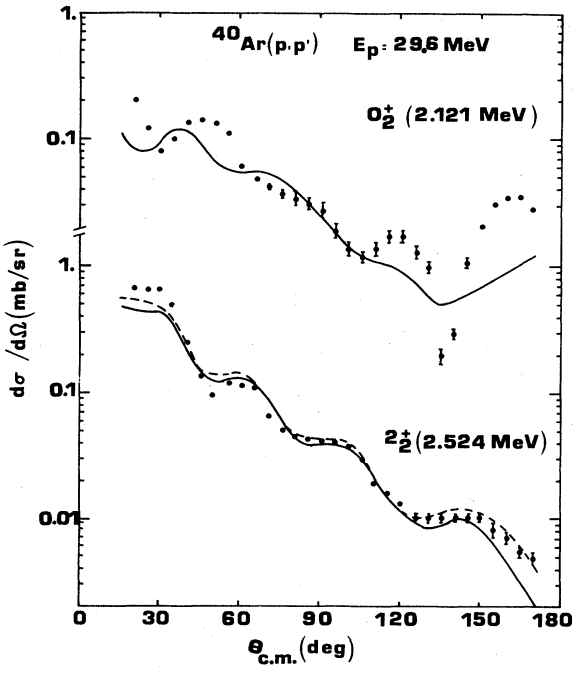

FIG. 5. Cross sections of the 0_2^+ and 2_2^+ levels of ^{40}Ar at the incident proton energy of 29.6 MeV. Full curves refer to a coupled channel calculation with first derivative ($\lambda = 2,4$) and Satchler ($\lambda = 0$) form factors, and $B(E\lambda)$ values from the seventh column of Table V; the 0_1^+, 2_1^+, 0_2^+, and 2_2^+ levels have been coupled. The dashed line refers to a similar analysis with the 0_2^+ level omitted from the coupling scheme and with $B(E\lambda)$ values from the eighth column of Table V.

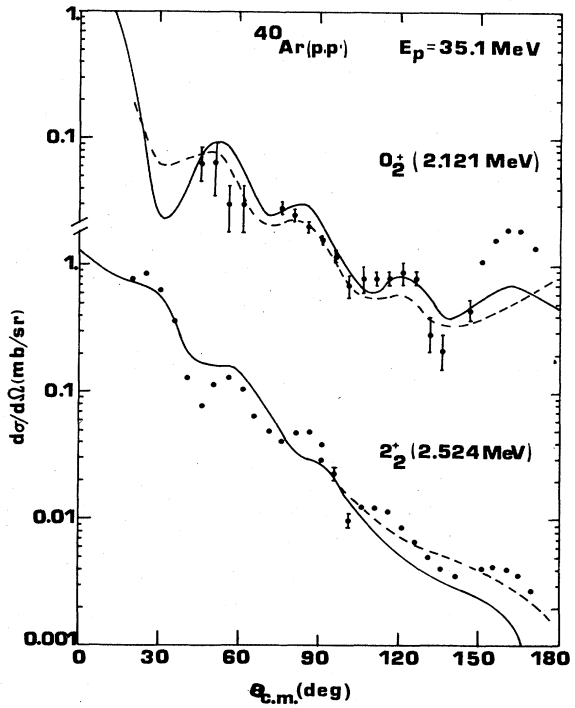

FIG. 6. Cross sections of the 0_2^+ and 2_2^+ levels of ^{40}Ar at the incident proton energy of 35.1 MeV. The full curves are the results of a rotor-vibrator model analysis, coupling the 0_1^+, 2_1^+, 0_2^+, and 2_2^+ levels. The long-dashed curve refers to a coupled channel calculation with first derivative ($\lambda = 2,4$) and Satchler ($\lambda = 0$) form factors, and $B(E\lambda)$ values from the seventh column of Table V; the 0_1^+, 2_1^+, 0_2^+, and 2_2^+ levels have been coupled. The short-dashed line refers to a similar analysis with the 0_2^+ level omitted from the coupling scheme and with $B(E\lambda)$ values from the eighth column of Table V.

2_2^+ cross sections are of the same quality as the previous ones, a result that confirms the conclusions of the analysis reported in Fig. 4 with short-dashed lines and indicates that the absence of the coupling to the 0_2^+ level can be easily compensated for with those from the other levels. In fact, the sign of the multipole moment $M(E2,0_1^+ \rightarrow 2_2^+)$ so obtained is reversed with respect to that from all previous analyses (see Table V). Therefore it is obvious that for a correct evaluation of the multipole moments from hadron scattering it is important to perform CC calculations with the appropriate coupling scheme. Only then a good comparison with values from em decay studies is possible.

V. THE 3_1^- LEVEL

The experimental cross sections for the 3_1^- level at 3.681 MeV are displayed in Fig. 7. This level is nicely reproduced by a simple distorted wave Born approximation (DWBA) requiring a deformation parameter $\beta_3 = 0.26$ (Table II). The curves are shown in Fig. 7.

In the following the influence of coupled channels on this level will be considered. Looking at the γ-decay scheme in Table III one notes that this state decays strongly to the 2_1^+ level. The transition is, however, predominantly electric dipole in character. The 3_1^- state decays also to the 2_2^+ and 4_1^+ states, presumably also with electric dipole transitions. It is fed[6] from an upper 4^- state at 4.226 MeV (decay not shown in Table III). Unfortunately, there is no chance to resolve the 4^- state in the present experiment; but since it cannot be excited directly from the g.s. its omission from the coupled-channels level scheme should not significantly influence the evaluated 3_1^- cross section. Considering also that the cross sections of the 2_2^+ and 4_1^+ levels are one order of magnitude smaller than that of the 2_1^+, it seems plausible to couple only the 0_1^+, 2_1^+ states to the 3_1^- level. Assuming first derivative form factors and searching on all the multipole moments, we obtained fits very similar to the full lines of Fig. 7 and therefore did not report them. The obtained $B(E\lambda)$ values are instead reported in the fourth column of Table VI. The $B(E3,0_1^+ \rightarrow 3_1^-)$ values deduced from the DWBA and CC analyses are very similar.

TABLE VI. $B(E\lambda)$ values in $e^2\text{fm}^{2\lambda}$ from the (p,p') analyses described in Sec. V.

$J_i \rightarrow J_f$	λ	$B(E\lambda)$(p,p')[a]	$B(E\lambda)$(p,p')[b]
$0_1^+ \rightarrow 3_1^-$	3	-15030 ± 460	-16531 ± 330
$2_1^+ \rightarrow 3_1^-$	3		-3803 ± 980
$2_1^+ \rightarrow 3_1^-$	5		$(-3.5 \pm 1.7) \times 10^5$

[a]From a DWBA analysis.
[b]From a fit on the rme's. First derivative ($\lambda = 2,3,5$) form factors. 0_1^+, 2_1^+ and 3_1^- levels coupled.

VI. OTHER 2^+ STATES

The experimental cross sections for the excitation of two 2^+ states at 3.208 and 3.919 MeV are given in Figs. 8 and 9. The first level is of particular interest since it should be produced by the coupling of the ^{42}Ca g.s. with

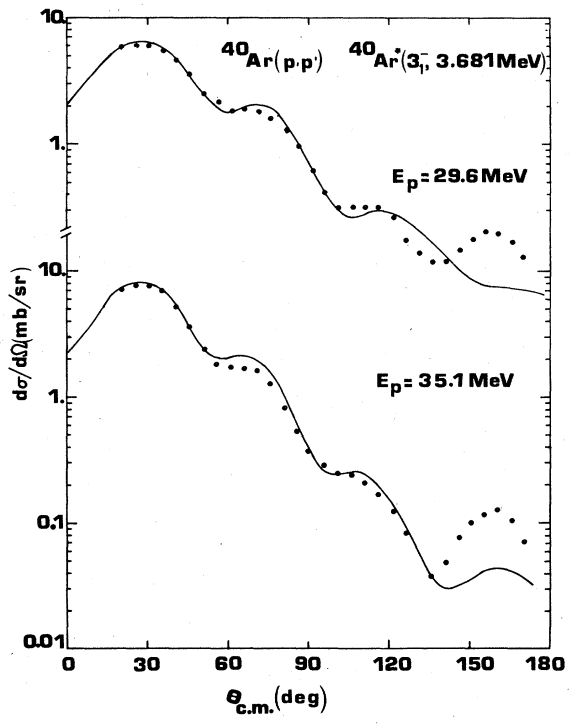

FIG. 7. Cross sections of the 3_1^- level of ^{40}Ar at the quoted proton incident energies. The curves are the results of a DWBA analysis.

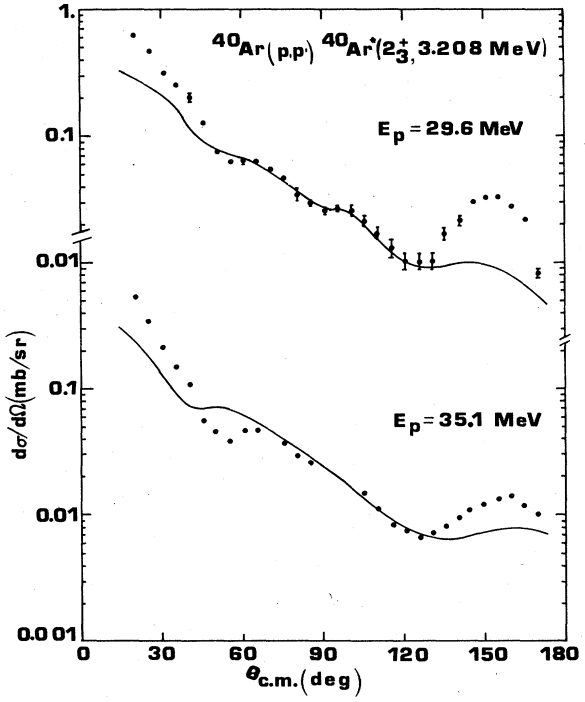

FIG. 8. Cross sections of the 2_3^+ level of ^{40}Ar at the quoted proton incident energies. The curves are the results of a coupled channel calculation obtained coupling the 0_1^+, 2_1^+, and 2_3^+ levels and using the $B(E\lambda)$ values in the fifth column of Table VII.

TABLE VII. $B(E\lambda)$ values in $e^2fm^{2\lambda}$ from γ-decay experiments and from the (p,p') analyses described in Sec. VI.

$J_i \rightarrow J_f$	λ	$B(E\lambda)$(em)[a]	$B(E\lambda)$(em)[b]	$B(E\lambda)$(p,p')[c]
$0_1^+ \rightarrow 2_3^+$	2	29±6	30±15	10±3
$2_1^+ \rightarrow 2_3^+$	2	12±5	13±9	14±5
$2_1^+ \rightarrow 2_3^+$	4			39 735±34 330
$0_1^+ \rightarrow 2_4^+$	2	6±1	7±1	24±2
$2_1^+ \rightarrow 2_4^+$	2	>0.3, <3.3	>0.4, <4.1	65±29
$2_1^+ \rightarrow 2_4^+$	4			104 950±16 700

[a]Deduced from Ref. 14.
[b]Deduced from Ref. 6.
[c]From a fit on the rme's. First derivative ($\lambda=2,4$) form factors. 0_1^+, 2_1^+, and 2_i^+ levels coupled.

two $d_{3/2}$ proton holes coupled to $L=2$. In fact its experimental cross sections resemble more those of the elastic cross sections rather than those of a 2^+ state such as those of the 2_4^+ state. Also the γ decay of the 2_3^+ state is different from that of the 2_4^+ state (see Table III). The 2_3^+ state decays only to the 0_1^+ and 2_1^+ g.s. band levels, while the 2_4^+ is also linked to the 0_2^+ and 2_2^+ states of the β band.

For the analysis of these two states we have assumed the 0_1^+, 2_1^+, and 2_i^+ level coupling scheme and first derivative form factors. Here i refers to either the third or the fourth 2^+ levels. The simplification of the level scheme for the 2_4^+ may result in a wrong determination of $B(E\lambda)$ values. The results of these analyses are shown in Figs. 8 and 9, and the $B(E\lambda)$ values are reported in Table VII. Good agreement exists between the $B(E\lambda)$ values from (p,p') and (em) experiments only for the 2_3^+ level. The disagreement between the $B(E2,2_1^+ \rightarrow 2_4^+)$ values may reflect the aforementioned simplified level coupling scheme.

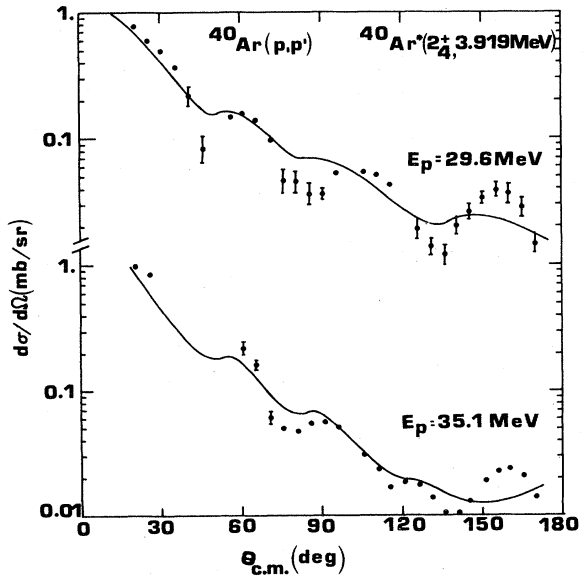

FIG. 9. Data and curves same as in Fig. 8 but for the 2_4^+ level.

VII. CONCLUSIONS

The differential cross sections from many excited states of ^{40}Ar have been measured at the incident proton energies of 29.6 and 35.1 MeV. The cross sections of the 0_1^+, 2_1^+, and 4_1^+ levels have been successfully reproduced using both the vibrational and the rotational model. Only slight differences in the values of the parameters of the two models have been found. The vibrational model analysis shows that the 4_1^+ state results mostly from a one-step hexadecapole one-phonon component rather than from a two-step two quadrupole phonons component. In analogy, in the rotational model, a strong hexadecapole deformation is necessary to reproduce the cross section of the level. The $B(E\lambda)$(p,p') values deduced for these levels are more reliable than those for higher energy states since for these levels the coupling scheme to be used in the coupled channel calculations is more obvious. The comparison of the deduced $B(E\lambda)$ values with the corresponding ones from γ-decay studies indicates that the $B(E2,0_1^+ \rightarrow 2_1^+)$ value obtained from em measurements is smaller; thus the neutron contribution seems greater than that of the protons for the excitation of this state. The result is moreover in agreement with the hypothesis of similarity in the level structure of the first excited states of ^{42}Ca and ^{40}Ar, and thus with the hypothesis that also the first states of the latter nucleus are due to the recoupling of two neutrons in the $f_{7/2}$ shell.

The 0_2^+ and 2_2^+ levels have been analyzed in Sec. IV. These levels have been considered as belonging to the β band. If the $0_2^+ \rightarrow 2_2^+$ coupling is ignored, an anomalously large quadrupole vibration amplitude (80% of the g.s. quadrupole deformation parameter) is found, even larger than that in ^{12}C (57%, Ref. 9). Including this coupling a value of 23% results, comparable with that of ^{24}Mg (18%, Ref. 8). In both cases a very weak mixing of the compressional mode (giant monopole resonance) in the 0_2^+ state was found necessary to reproduce the data. The strength of the $0_2^+ \rightarrow 2_2^+$ coupling is linked to the intrinsic quadrupole moment of the β band. A value of $Q_0=988\pm90$ e mb has been extracted, in agreement with that found in the literature (Ref. 6) and deduced from the $4_2^+ \rightarrow 2_2^+$ and $6_2^+ \rightarrow 4_2^+$ γ-decay transitions. A higher value,

$Q_0 = 1521 \pm 444$ e mb, but in relative agreement with the others, has been evaluated from our data in an analysis where all coupling amplitudes were considered as free parameters. The agreement among all the determined values for Q_0 of the β band confirms the hypothesis of the presence of deformed states in ^{40}Ar.

For the 3_1^- level equivalent fits have been obtained from a simple DWBA analysis and a more complex CC analysis. The results suggest a vibrational character for this band. The 2_3^+ and 2_4^+ cross sections have been reproduced with coupled channel calculations. The $B(E\lambda)$'s deduced for the first of these levels are in agreement with the electromagnetic ones. From the analysis of the latter level, strong $\lambda = 2,4$ two-step (through the 2_1^+ level) contributions have been found. The deduced $B(E2)$ values are in disagreement with those from electromagnetic studies and suggest a more complex level coupling scheme for this level.

[1]R. W. Bauer, A. M. Bernstein, G. Heymann, E. P. Lippincott, and N. S. Wall, Phys. Lett. **14**, 129 (1965).

[2]W. J. Gerace and A. M. Green, Nucl. Phys. **A93**, 110 (1967).

[3]P. Betz, H. Ropke, F. Glatz, G. Hammel, V. Glattes, and W. Brender, Z. Phys. **271**, 195 (1974).

[4]P. Betz, E. Bitterwolf, B. Busshardt, and H. Ropke, Z. Phys. A **276**, 295 (1976).

[5]Th. Kern, P. Betz, E. Bitterwolf, F. Glatz, and H. Ropke, Z. Phys. A **294**, 51 (1980).

[6]E. Bitterwolf, A. Bukard, P. Betz, F. Glatz, F. Heidinger, Th. Kern, R. Lehmann, S. Norbert, H. Ropke, C. Schneider, and J. Siefert, Z. Phys. A **313**, 123 (1983).

[7]T. Tamura, Rev. Mod. Phys. **37**, 679 (1965).

[8]M. N. Harakeh and R. De Leo, Phys. Lett. **117B**, 377 (1982).

[9]R. De Leo, G. D'Erasmo, A. Pantaleo, M. N. Harakeh, E. Cereda, S. Micheletti, and M. Pignanelli, Phys. Rev. C **28**, 1443 (1983).

[10]M. N. Harakeh, the code BEL, Kernfysisch Versneller Instituut Report No. 77i, 1981; K. van der Borg, M. N. Harakeh, and B. S. Nilsson, Nucl. Phys. **A325**, 31 (1979).

[11]R. De Leo *et al.* (unpublished).

[12]E. Fabrici, S. Micheletti, M. Pignanelli, F. G. Resmini, R. De Leo, G. D'Erasmo, A. Pantaleo, J. L. Escudiè, and A. Tarrats, Phys. Rev. C **21**, 830 (1980).

[13]J. Raynal, the code ECIS, private communication.

[14]P. M. Endt and C. van der Leun, Nucl. Phys. **A310**, 1 (1978).

[15]J. R. Southon, A. R. Poletti, and D. J. Beale, Nucl. Phys. **A267**, 263 (1983).

[16]A. M. Bernstein, V. R. Brown, and V. A. Madsen, Phys. Rev. Lett. **42**, 425 (1979).

[17]G. R. Satchler, Nucl. Phys. **A100**, 481 (1967); Part. Nucl. **5**, 107 (1972).

[18]B. Castel and G. R. Satchler, Phys. Lett. **80B**, 13 (1978).

[19]H. P. Morsch, Phys. Lett. **61B**, 15 (1976); H. P. Morsch and P. Decowski, *ibid.* **82B**, 1 (1979).

[20]K. van der Borg, M. N. Harakeh, and A. van der Woude, Nucl. Phys. **A365**, 243 (1981); T. Yamagata, K. Iwamoto, S. Kishimoto, B. Saeki, K. Yuasa, M. Tanaka, T. Fukuda, K. Ogata, I. Miura, M. Inone, and H. Ogata, Phys. Rev. Lett. **40**, 1628 (1978); D. L. Lebrun, M. Buenerd, P. Martin, P. de Saintignon, and G. Perrin, Phys. Lett. **97B**, 358 (1980).

[21]P. D. Kunz, the code CHUCK, University of Colorado (unpublished).